Fizika Nizkikh Temperatur, 2004, v. 30, No. 4, p. 355–372

Advances in point-contact spectroscopy: two-band superconductor MgB_2

(Review Article)

I.K. Yanson and Yu.G. Naidyuk

B.Verkin Institute for Low Temperature Physics and Engineering of the National Academy of Sciences of Ukraine, 47 Lenin Ave., Kharkov 61103, Ukraine
E-mail: yanson@ilt.kharkov.ua

Received July 28, 2003

Analysis of the point-contact spectroscopy (PCS) data on the new dramatic high-T_c superconductor magnesium diboride MgB_2 reveals quite different behavior of two disconnected σ and π electronic bands, deriving from their anisotropy, different dimensionality, and electron–phonon interaction. PCS allows direct registration of both the superconducting gaps and electron–phonon interaction spectral function of the two-dimensional σ and three-dimensional π band, establishing correlation between the gap value and intensity of the high-T_c driving force — the E_{2g} boron vibration mode. PCS data on some nonsuperconducting transition-metal diborides are surveyed for comparison.

PACS: 74.25.Fy, 74.80.Fp, 73.40.Jn

Contents

1. Introduction

MgB_2 was discovered to be superconducting only a couple of years ago [1], and despite that, many of its characteristics have now been investigated and a consensus exists about its outstanding properties. First of all, this refers to its high T_c (≈ 40 K) which is a record-breaking value among the $s-p$ metals and alloys. It appears that this material is a rare example of

multiband (at least two) electronic structure, which are weakly connected with each other. These bands lead to very uncommon properties. For example, T_c is almost independent of elastic scattering, unlike for other two-band superconductors [2]. The maximal upper critical magnetic field can be made much higher than that for a one-band dirty superconductor [3]. The properties of MgB_2 have been comprehensively calculated by the modern theoretical methods, which lead to a basic understanding of their behavior in various experiments.

1.1. Crystal structure

Magnesium diboride, like other diborides MeB_2 (Me = Al, Zr, Ta, Nb, Ti, V etc.), crystalizes in a hexagonal structure, where honeycomb layers of boron are intercalated with hexagonal layers of magnesium located above and below the centers of boron hexagons (Fig. 1). The bonding between boron atoms is much stronger than that between magnesium, and therefore the disordering in the magnesium layers appears to be much easier than in the boron layers. This difference in bonding between boron and magnesium atoms hinders the fabrication of MgB_2 single crystals of appreciable size.

1.2. Electron band structure

The electron band structure of MgB_2 has been calculated using different *ab initio* methods yielding basically the same result [4–8]. The $E(k)$ curves are shown in Fig. 2. The dispersion relations are shown for boron *p*-character orbitals, which play a major role in transport and thermodynamic properties. The radii of the hollow circles are proportional to the π-band character, which is made from p_z boron orbitals, while those of the filled circles are proportional to the σ-band character, made from p_{xy} orbitals. The most important is a quasi-two-dimensional dispersion relation along the ΓA (Δ) direction with a small Fermi energy ≈ 0.6 eV, and accordingly, with a moderate Fermi velocity. The corresponding sheets of the Fermi energy form the cylindrical surfaces along the ΓA direction seen in Fig. 5 below. The corresponding electron transport is very anisotropic ($\rho_c/\rho_{ab} \simeq 3.5$ [10]), with the plasma frequency for the σ band along the *c* (or *z*) axis being much smaller than that in the *ab* (*xy*) direction [11]. The hole branch along ΓA experiences a huge interaction with the phonon E_{2g} mode for carriers moving along the *ab* plane (see below), although its manifestation is screened effectively by the much faster hole mobility in the π band [2].

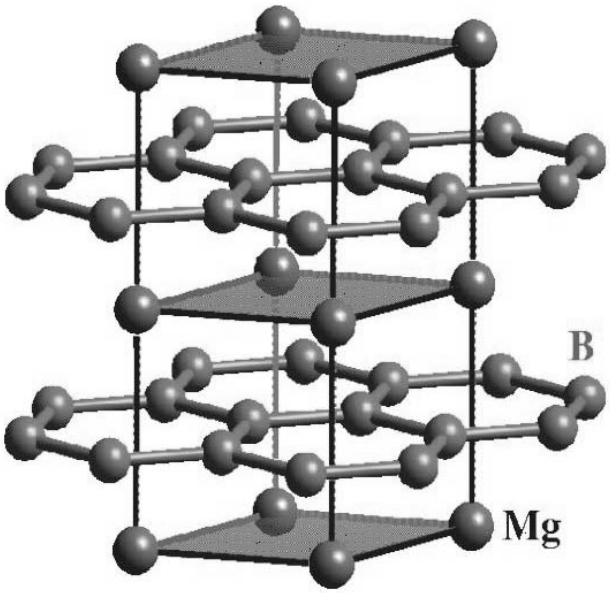

Fig. 1. Crystal structure of MgB_2.

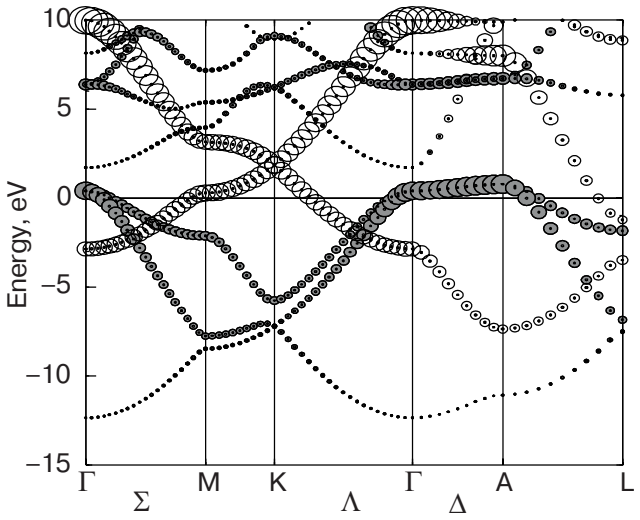

Fig. 2. Band structure of MgB_2 with the B *p* character. The radii of the hollow (filled) circles are proportional to the π (σ) character and zero-line marks the Fermi energy. After Mazin et al. [9].

In a dirty material, with prevailing disorder in the magnesium planes, the π-band conductivity is blocked by defects, and the σ band takes over, implying greater electron–phonon interaction (EPI) than in the clean material. This constitutes a plausible explanation for the violation of the Matthiesen rule, which manifests itself in an increase of the residual resistivity together with an increase of the temperature coefficient at high temperatures [2].

At the same time, the critical temperature T_c does not decrease substantially in dirty materials [2], since

the superconductivity is induced by EPI in the σ band, whose crystal order is much more robust.

This consideration is very important in understanding the point-contact data, since the disorder at the surface of the native sample depends on the position of the contact spot, and because of the uncontrolled introduction of further disorder while fabricating the contact.

1.3. Critical magnetic field

In a clean material the layered crystal structure dictates strong anisotropy of the upper critical magnetic fields $B_{c2}^{ab} >> B_{c2}^{c}$. Their ratio at low temperatures reaches about 6 while B_{c2}^{c} is as low as 2–3 T [12]. If the magnetic field is not aligned precisely along the *ab* plane, the B_{c2} value is strongly decreased.

On the other hand, for a dirty material the anisotropy is decreased (to a ratio of about 1.6–2), but both the magnitudes of B_{c2}^{ab} and B_{c2}^{c} are strongly increased. For strongly disordered sample, it may be as high as 40 T [3]! It is interesting that this high value is achieved at low temperature, where the disordered π band is fully superconducting.

Hence, we may expect that the value of the critical magnetic field at low temperatures is the smaller the cleaner is the part of the MgB_2 volume near the contact, provided its $T_c \simeq T_c^{\text{bulk}}$. This observation is important in the classification of contacts with respect to their purity.

1.4. Phonons and electron–phonon interaction

The phonon density of states (PDOS) is depicted in Fig. 3. The upper panel shows the measured PDOS at $T = 8$ K, while the lower ones show the calculated DOS with the partial contribution from boron atoms moving in the *ab* plane and out of it. One can see the peak for boron atoms moving in the *ab* plane at $\simeq 75$ meV, which plays a very important role in the electron–phonon interaction, as is shown in Fig. 4, measured by inelastic x-ray scattering [14]. This mode gives a weakly dispersion branch between 60 and 70 meV in the ΓA direction with E_{2g} symmetry at the Γ point. The linewidth of this mode is about 20–28 meV along the ΓA direction, while along the ΓM direction it is below the experimental resolution. The same phonon peak is active in Raman scattering [15–17]. It is located at the same energy with the same linewidth. This points to the very strong EPI for this particular lattice vibration mode. The same result follows from theoretical considerations.

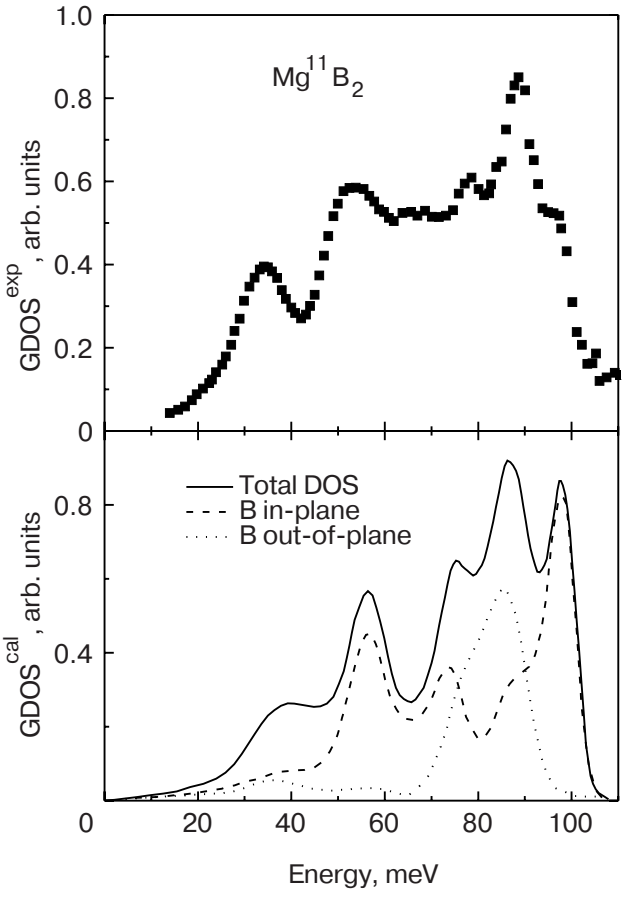

Fig. 3. Upper panel: Phonon density of states in MgB_2 determined experimentally by neutron scattering. Bottom panel: calculated curve (solid line) with decomposition on boron atoms vibrating out of *ab* plane (dotted curve) and parallel to it (dashed curve). After Osborn et al. [13].

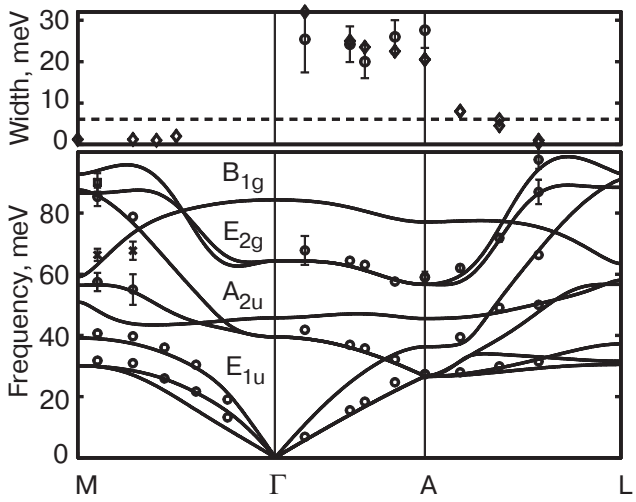

Fig. 4. Dispersion curves of phonons in MgB_2 and the width of phonon lines determined by inelastic x-ray scattering (symbols) together with calculations (solid lines). After Shukla et al. [14].

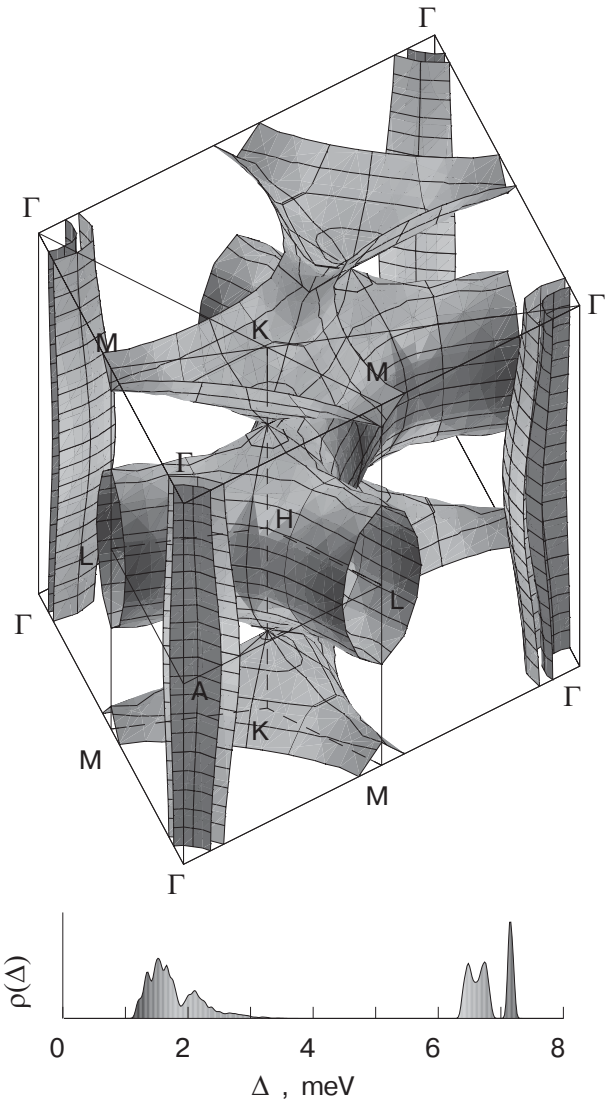

Fig. 5. Superconducting energy gap distribution over the Fermi surface (FS) of MgB_2. The gap value around 7 meV corresponds to cylinderlike sheets of the FS centered at Γ points, while the small gap value around 2 meV corresponds to the tubular FS network. After Choi et al. [18].

Figure 5 shows the distribution of the superconducting energy gap on the Fermi surface of MgB_2 [18]. The maximum gap value is calculated along the ΓA direction due to the very strong EPI. Just in this direction is located 2D σ band (cylinders along the ΓA direction). The 3D π band has a much smaller EPI, and, correspondingly, a smaller energy gap. The EPI parameter λ can be decomposed between different pieces of the Fermi surface. It is shown [19] that the value of λ on the σ band amounts to 2–3. Moreover, λ_σ can be decomposed between different phonon modes, and it appears that only the E_{2g} phonon mode along the ΓA direction plays a major role with a partial λ_σ value of about $\simeq 25$ [20], though concentrated in a very restricted phase space.

1.5. Mechanism for high T_c in MgB_2

The commonly accepted mechanism for high T_c in MgB_2 is connected with the strong interaction between charge carriers and phonons in the E_{2g} mode.This mode is due to antiparallel vibration of atoms in the boron planes. The key issue is that along the ΓA direction the electron band structure is such that the Fermi energy of the hole carriers is only 0.5–0.6 eV, which shrinks even more when the borons deviate from the equillibrium positions. Together with the 2D structure of the corresponding sheet of the Fermi surface, this leads to a constant density of states at the Fermi energy and, correspondingly, to very large EPI with partial λ_σ (the EPI parameter in the σ band) of about ~ 25 [20]. Cappelluti et al. [21] point out that the small Fermi velocity for charge carriers along the ΓA direction leads to a large nonadiabatic correction to T_c (about twice as much compared with the adiabatic Migdal–Eliashberg treatment). Although this interaction is a driving force to high T_c in this compound, it does not lead to crystal structure instability, since it occupies only a small volume in the phase space.

The role of the π band is not completely clear. On the one hand, the π and σ bands are very weakly connected, and for some crude models they can be thought as being completely disconnected. On the other hand, the energy gap of the π band goes to zero at the same T_c as in the bulk, and correspondingly $2\Delta_\pi(0)/kT_c = 1.4$, which is much less than the value predicted by the weak-coupling BCS theory. One can think of the π band as having intrinsically much lower $T_c \approx 10$ K than the bulk [22], and at higher temperatures its superconductivity is induced by a proximity effect in **k** space from the σ band [23]. This proximity effect is very peculiar. On the one hand, this proximity is induced by the interband scattering between the π and σ sheets of the Fermi surface. On the other, the charge carriers connected with the π band are mainly located along the magnesium planes, which can be considered as a proximity effect in coordinate space for alternating layers of $S-N-S$ structure, although on a microscopic scale. Moreover, many of the unusual properties of MgB_2 may be modeled by an alternating $S-N-S$ layer structure, the limiting case to the crystal structure of MgB_2. In other words, MgB_2 presents a crossover between two-band superconductivity and a simple proximity-effect structure.

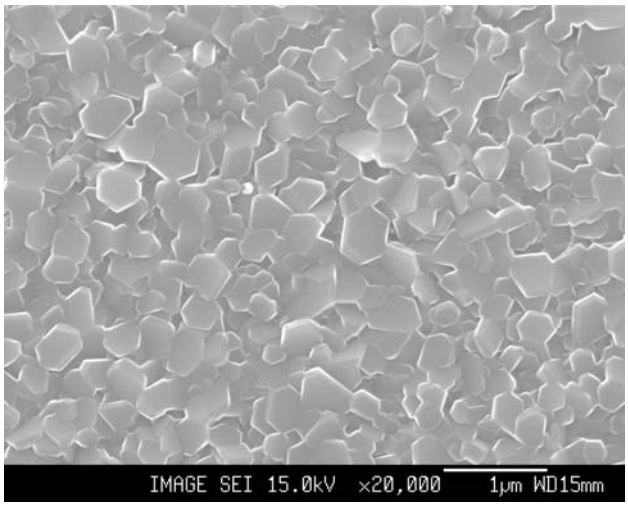

Fig. 6. Scanning electron microscopy image of MgB_2 films. After Kang et al. [25].

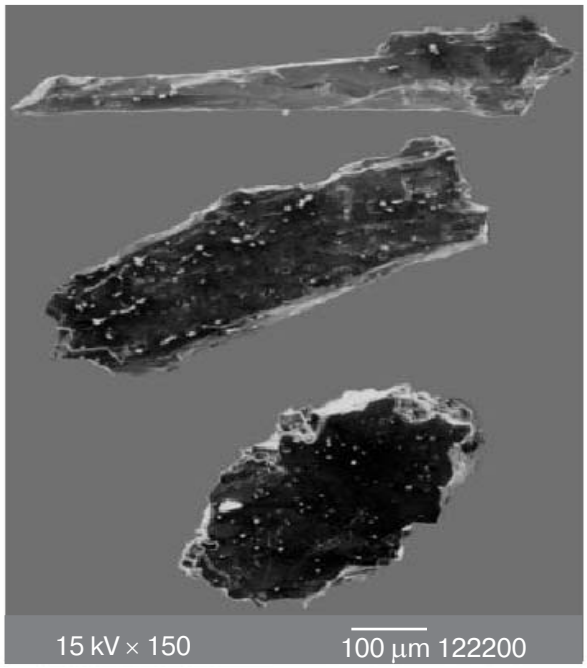

Fig. 7. Scanning electron microscopy image of MgB_2 single crystals. After Lee et al. [26].

2. Samples

We have two kind of samples supplied for us by our colleagues from the Far East*.

The first is a thin film with a thickness of about several hundred nanometers (Fig. 6) [24]. Similar films have been investigated by several other groups with different methods. These films are oriented with their *c* axis perpendicular to the substrate. The residual resistance is about several tens of $\mu\Omega \cdot$ cm with a residual resistance ratio (RRR) $\simeq 2.2$. This means that on average the films have a disorder between crystallites.

It does not exclude the possibility that on some spots the films contain clean enough small single crystals on which we occasionally may fabricate a point contact; see Fig. 6. Normally, we make a contact by touching the film surface by noble metal counter electrode (Cu, Au, Ag) in the direction perpendicular to the substrate. Thus, nominally the preferential current direction in the point contact is along the *c* axis. Nevertheless, since the surface of the films contains terraces with small crystallites, point contact to the *ab* plane of these crystallites is also possible. Sometimes, in order to increase the probability of making the contact along the *ab* plane, we broke the substrate with the film and made contact to the side face of the sample.

The second type of sample is single-crystal [26], which also was measured by other groups [10,27]. Crystals are platelike (flakes) and have submillimeter size (see Fig. 7). They were glued by silver epoxy to the sample holder by one of their side faces. The noble metal counter electrode was gently touched in liquid helium by another (the opposite) side face of the crystal. In this way we try to preferentially make a contact along the *ab* plane. On average, in the bulk, the single crystals are cleaner than the films, but one should be cautious, since the properties of the crystal surface differ from the properties of the bulk, and fabrication of a point contact may introduce further uncontrolled defects into the contact area.

Thus, *a priori* one cannot define the structure and composition of the contacts obtained. Nevertheless, much of that information can be ascertained by measuring various characteristics of a contact. Among those the most important is the Andreev-reflection nonlinearities of the $I-V$ curves in the superconducting energy-gap range. The magnetic-field and temperature dependences of the superconducting nonlinearities supply us with additional information. And finally, much can be extracted from the $I-V$ nonlinearities in the normal states (the socalled point-contact spectra). The more information we can collect about the electrical conductivity for different

* The films were provided by S.-I. Lee from National Creative Research Initiative Center for Superconductivity, Department of Physics, Pohang University of Science and Technology, Pohang, South Korea. The single crystals were provided by S. Lee from Superconductivity Research Laboratory, ISTEC, Tokyo, Japan.

conditions of the particular contact, the more detailed and defined picture of it emerges. It is not an easy task, since a contact has limited lifetime, due to electrical and mechanical shocks.

Let us make a rough estimate of the distance scales involved in the problem. The crystallite size of the films is of the order of 100 nm (see [25]). The contact size d in the ballistic regime equals $d \simeq \sqrt{\rho l / R}$ (the Sharvin formula). Taking $\rho l \cong (7 \cdot 10^{-7}\ \Omega \cdot \text{cm})(7 \cdot 10^{-6}\ \text{cm}) = 4{,}9 \cdot 10^{-12}\ \Omega \cdot \text{cm}^2$ [10], we obtain $d \simeq 7$ nm along both the *ab* and *c* directions for a typical resistance of 10 Ω. If we suppose that a grain is dirty (with a very short mean free path), then we apply the Maxwell formula $d \sim \rho / R$ with the results for d values of about 0.7 nm and 2.6 nm for the *ab* and *c* directions, respectively, taking ρ for the corresponding directions from the same reference [10]. Thus, the contact size can be of the order of or smaller than the electronic mean free path ($l_{ab} = 70$ nm and $l_c = 18$ nm, according to [10]), which means that we are working admittedly in the spectroscopic regime, probing only a single grain.

Rowell [28], analyzing a large amount of experimental data for the resistivity and its temperature dependence, came to the conclusion that for highly resistive samples only a small part of the effective cross section should be taken into account. The reason is that the grains in MgB_2 are to great extent disconnected by oxides of magnesium and boron. For point-contact spectroscopy previous analysis leads us to the conclusion that the contact resistance is frequently measured only for a single grain or for several grains, with their intergrain boundaries facing the contact interface. This is due to the current spreading on a scale of the order of the contact size d near the constriction.

3. Theoretical background of PCS

3.1. Nonlinearity of I–V characteristic

The nonlinearities of the I–V characteristic of a metallic contact, when one of the electrodes is in the superconducting state, can be written as [29,30]

$$I(V) \simeq \frac{V}{R_0} - \delta I_{\text{ph}}^{N}(V) + I_{\text{exc}}(V)\ . \qquad (1)$$

Here R_0 is the contact resistance at zero bias in the normal state. $\delta I_{\text{ph}}^{N}(V)$ is the backscattering inelastic current, which depends on the electron mean free path (mfp) l. For ballistic contact this term is equal in order of magnitude to

$$\delta I_{\text{ph}}^{N}(V) \sim \frac{d}{l_{\text{in}}} I(V)\ , \qquad (2)$$

where l_{in} is the inelastic electron mfp, and d is the characteristic contact diameter. If the electron flow through the contact is diffusive ($l_{\text{el}} << d$, l_{el} being an elastic mfp) but still spectroscopic, since $\sqrt{l_{\text{in}} l_{\text{el}}} >> d$, then the expression (2) should be multiplied by l_{el}/d. This decreases the characteristic size for which the inelastic scattering is important from d to l_{el} ($d \to l_{\text{el}}$), and for short l_{el} makes the inelastic current very small. We notice that the inelastic backscattering current $\delta I_{\text{ph}}^{N}(V)$ in the superconducting state is approximately equal to the same term in the normal state. Its second derivative turns out to be directly proportional to the EPI function $\alpha^2(\omega)\, F(\omega)$ [31,32]

$$-\frac{d^2 I}{dV^2} \propto \frac{8ed}{3\hbar v_F} \alpha^2(\omega)\, F(\omega) \qquad (3)$$

where α describes the strength of the electron interaction with one or another phonon branch, and $F(\omega)$ stands for the phonon density of states. In point-contact (PC) spectra the EPI spectral function $\alpha^2(\omega)\, F(\omega)$ is modified by the transport factor, which strongly increases the backscattering processes contribution.

In the superconducting state the excess current I_{exc} (1), which is due to the Andreev reflection of electron quasiparticles from the N–S boundary in an N–c–S point contact (c stands for «constriction»), can be written as

$$I_{\text{exc}}(V) = I_{\text{exc}}^{0} + \delta I_{\text{exc}}(V) \qquad (4)$$

where $I_{\text{exc}}^{0} \approx \Delta / R_0 \approx \text{const}$ for $eV > \Delta$ (Δ being the superconducting energy gap).

The nonlinear term in the excess current (4) can in turn be decomposed in two parts, which depend in different ways on the elastic scattering of electron quasiparticles:

$$\delta I_{\text{exc}}(V) = \delta I_{\text{exc}}^{\text{el}}(V) + \delta I_{\text{exc}}^{\text{in}}(V) \qquad (5)$$

where $\delta I_{\text{exc}}^{\text{el}}(V)$ is of the order of $(\Delta/eV) I_{\text{exc}}^{0}$, and $\delta I_{\text{exc}}^{\text{in}} V \sim (d/l_{\text{in}}) I_{\text{exc}}^{0}$. Notice that the latter behaves very similarly to the inelastic backscattering current $\delta I_{\text{ph}}^{N}(V)$, namely, it disappears if $l_{\text{el}} \to 0$, while the first term in the right-hand side of expression (5) does not depend on l_{el} in the first approximation. This enables one to distinguish the elastic term from the inelastic. Finally, all excess current terms disappear when the superconductivity is destroyed, while $\delta I_{\text{ph}}^{N}(V)$ remains very similar in both the superconducting and normal states.

The expression for the elastic term in the excess current was calculated for *ballistic* N–c–S contacts by Omelyanchuk, Beloborod'ko, and Kulik [33]. Its first derivative equals ($T = 0$):

$$\left(\frac{dI_{\rm exc}^{\rm el}}{dV}\right)_{NcS}^{\rm ballistic} = \frac{1}{R_0}\left|\frac{\Delta(eV)}{eV+\sqrt{(eV)^2-\Delta^2(eV)}}\right|^2. \quad (6)$$

For the *diffusive* limit ($l_i << d$), Beloborod'ko et al. derived the current–voltage characteristic (see Eq. (21) in Ref. 34), which for the first derivative at $T = 0$ gives [35]:

$$R_0\left(\frac{dI_{\rm exc}^{\rm el}}{dV}\right)_{NcS}^{\rm diffusive} = \frac{1}{2}\ln\left|\frac{eV+\Delta(eV)}{eV-\Delta(eV)}\right| \times$$

$$\times \mathrm{Re}\left[\frac{eV}{\sqrt{(eV)^2-\Delta^2(eV)}}\right] \Big/ \mathrm{Re}\left[\frac{\Delta(eV)}{\sqrt{(eV)^2-\Delta^2(eV)}}\right]. \quad (7)$$

For the sake of comparison, the similar expression of the nonlinear term in *NIS* tunnel junctions (*I* stands for «insulator»), due to the self-energy superconducting energy gap effect, has the form [36]:

$$\left(\frac{dI}{dV}\right)_{NIS} = \frac{1}{R_0}\mathrm{Re}\left[\frac{eV}{\sqrt{(eV)^2-\Delta^2(eV)}}\right]. \quad (8)$$

Equations (6), (7), and (8) are identical in their structure and take into account the same effect, viz., the renormalization of the energy spectrum of a superconductor in the vicinity of characteristic phonon energies.

From the expressions (1), (2), (4), and (5) it becomes clear that only on the relatively *clean* spots can one observe the inelastic backscattering current $\delta I_{\rm ph}^N(V)$, provided that the excess current term $\delta I_{\rm exc}^{\rm in}(V)$ is negligible. The latter can be canceled by suppression of superconductivity either with magnetic field or temperature. On the contrary, in the superconducting state, for *dirty* contacts, all the inelastic terms are very small, and the main nonlinearity is provided by the $\Delta(eV)$ dependence of the excess current (7).

3.2. Two-band anisotropy

Brinkman et al. have shown [11] that in the clean case for an *NIS* MgB_2 junction, the normalized conductance is given by

$$\sigma(V) = \left(\frac{dI}{dV}\right)_{NIS} \Big/ \left(\frac{dI}{dV}\right)_{NIN} = \frac{(\omega_p^\pi)^2\sigma_\pi(V) + (\omega_p^\sigma)^2\sigma_\sigma(V)}{(\omega_p^\pi)^2 + (\omega_p^\sigma)^2}$$

where $\omega_p^{\pi(\sigma)}$ is the plasma frequency for the $\pi(\sigma)$ band and $\sigma_{\pi(\sigma)}(V)$ is the normalized conductivity of the $\pi(\sigma)$ band separately. The calculated tunneling conductance in the *ab* plane and along the *c* axis are [11]

$$\sigma_{ab}(V) = 0.67\sigma_\pi(V) + 0.33\sigma_\sigma(V), \quad (10)$$

$$\sigma_c(V) = 0.99\sigma_\pi(V) + 0.01\sigma_\sigma(V). \quad (11)$$

Hence, even along the *ab* plane the contribution of the σ band is less than that of the π band, to say nothing about the direction along the *c* axis, where it is negligible small. The calculation predicts that if the «*tunneling cone*» is about several degrees from precise the *ab* plane, then the two superconducting gaps should be visible in the tunneling characteristics. In other directions only a single gap, corresponding to the π band, is visible. We will see below that this prediction is fulfilled in a point-contact experiment, as well.

Things are even worse when one tries to measure the anisotropic Eliashberg function by means of superconducting tunneling. The single-band numerical inversion program [36,37] gives an uncertain result, as was shown in Ref. 38.

Point-contact spectroscopy in the normal state can help in this deadlock situation. It is known that the inelastic backscattering current is based on the same mechanism as an ordinary homogeneous resistance, provided that the maximum energy of the charge carriers is controlled by an applied voltage. The electrical conductivity of MgB_2 can be considered as a parallel connection of two channels, corresponding to the π and σ bands [2]. The conductivity of the π band can be blocked by disorder of the Mg atoms . This situation is already obtained in experiment, when the temperature coefficient of resistivity increases simultaneously with an increase of the residual resistivity, which leads to

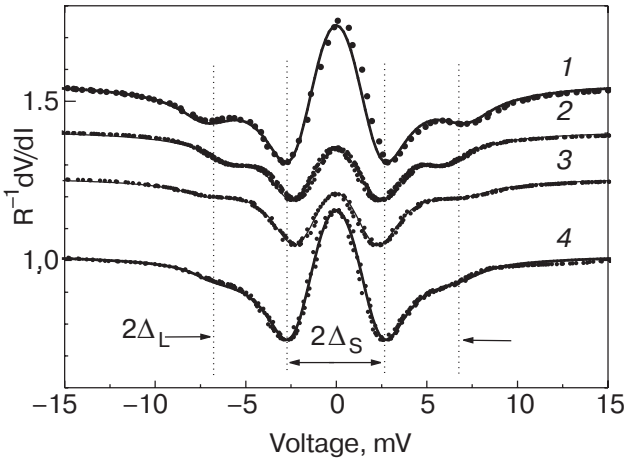

Fig. 8. Typical shapes of dV/dI (experimental dots) for 4 contacts between MgB_2 thin film and Ag with the corresponding BTK fitting (lines). $\Delta_{L(S)}$ stand for large (small) superconducting energy gap. After Naidyuk et al. [40].

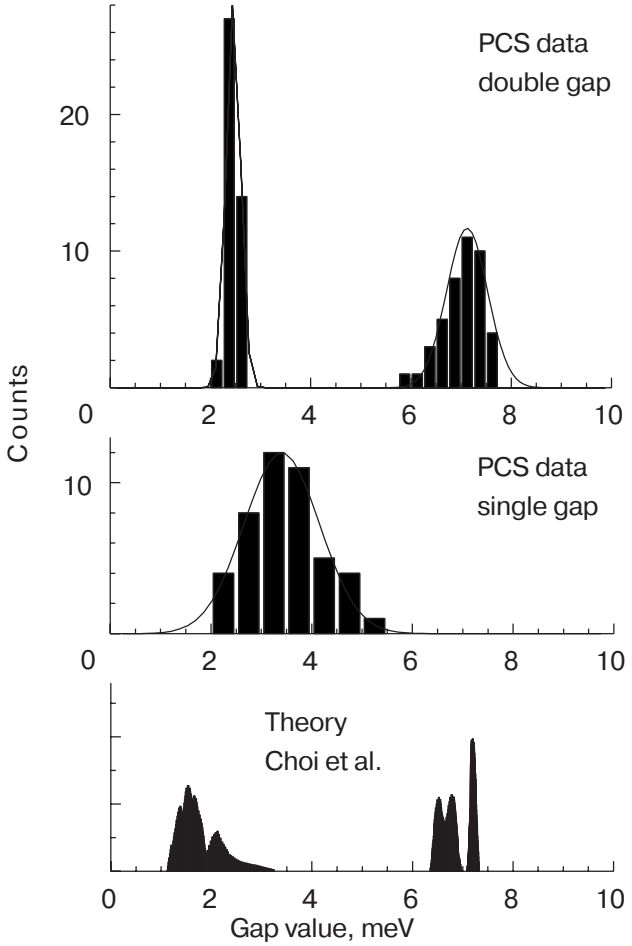

Fig. 9. Superconducting energy gap distribution of ~100 different junctions prepared on a MgB_2 film. On the lower panel the theoretical distribution is shown. After Naidyuk et al. [40].

violation of Matthiessen's rule (see Fig. 3 in [2]). In this case we obtain direct access to the σ-band conductivity, and the measurements of the PC spectra of the EPI for the σ band is explicitly possible in the normal state. Below we will see that this unique situation happens in single crystals along *ab* plane.

4. Experimental results

4.1. Superconducting energy gaps

c-axis oriented thin films. Our measurements of the superconducting energy gap by means of Andreev reflection from about a hundred *NS* junctions yield two kinds of dV/dI curves, shown in Fig. 8.

The first one clearly shows two sets of energy gap minima located, as shown in distribution graph of Fig. 9 (upper panel), at 2.4 ± 0.1 and (7.1 ± 0.4) meV. These curves are nicely fitted by BTK [39] theory (with small Γ parameter) for two conducting channels with an adjusted gap weighting factor [40]. The second kind is better fitted with a single gap provided an increased depairing parameter Γ (Fig. 9 (middle panel)). Certainly, the division of the gap structure into the two kinds mentioned is conventional, and depends upon the circumstance that the larger energy gap is explicitly seen. These two kinds of gap structure comprise about equal parts of the total number of junctions. Usually the contribution of the large gap in the double-gap spectra is an order of magnitude lower than that of the small one, which is in line with the small contribution of the σ band to the conductivity along the *c* axis (see Eq. (11)).

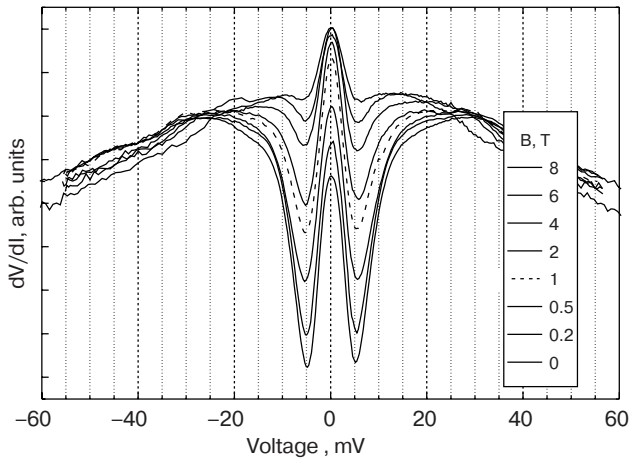

Fig. 10. Negative slope of dV/dI at large biases for a 36 Ω contact between MgB_2 single crystal and Ag showing the magnetic-field gap-structure evolution at 4.2 K.

It is important to note that the critical temperature of the material around the contact is not more than a few K below T_c in the bulk material. This is determined by the extrapolating the temperature dependence of PC spectra up to the normal state. Such an insensitivity of T_c on the elastic scattering rate is explained in Ref. 2. Nevertheless, we stress that the gap structure (either double- or single-gap feature, and the position of the single-gap minimum on dV/dI) depends very much on random variation of the scattering in the contact region. Moreover, since the main part of the junction conductivity is due to the charge carriers of the π band, even the background conductance quite often follows the «semiconductive» behavior, namely, the slope of the dV/dI curve at large biases is negative (Fig. 10). That means that the carriers in the π band are close to localization [41].

In the lower panel of Fig. 9 the theoretical prediction of the energy gap distribution [18] is shown. One can see that the theoretical positions of the distribution maxima coincide approximately with the experimental values. Only the low-lying maximum is not seen in the experiment. It should be noted that accord-

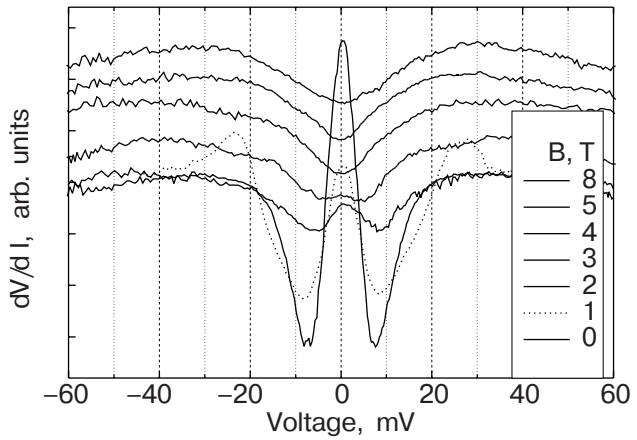

Fig. 11. Large gap structure evolution for single crystal MgB_2 – Au 87 Ω junction in magnetic field at 4.2 K. The curves are shifted vertically for clarity.

ing to Mazin et al. [42] variation of the superconducting gaps inside the σ and π bands can hardly be observed in real samples.

The distribution of the different gaps over the Fermi surface is shown in Fig. 5. One can immediately see that for a *c*-oriented film the main structure should have a smaller gap, which is approximately isotropic. Only if the contact touches the side face of a single crystallite (Fig. 6), is the larger gap visible, since it corresponds to the cylindrical parts of the Fermi surface with Fermi velocity parallel to the *ab* plane.

Single crystals. The same variety of energy gap structure is observed for single crystals as well, but with some peculiarity due to preferential orientation along the *ab* plane. The most amazing of them is the

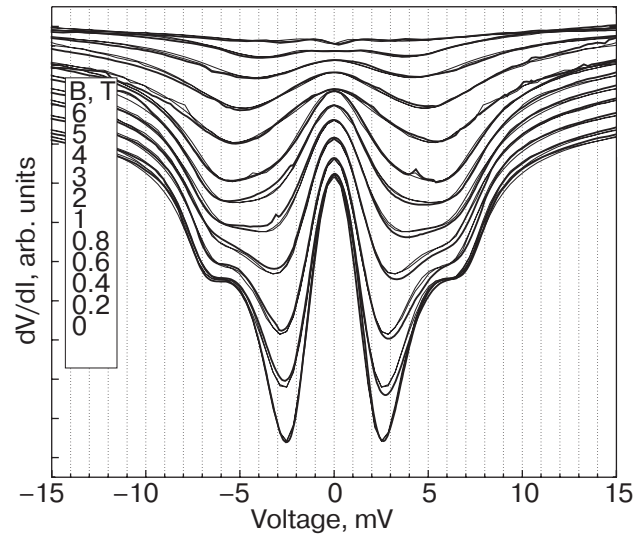

Fig. 12. Magnetic field dependences of dV/dI curves (solid lines) for a single-crystal MgB_2 – Cu 2.2 Ω junction along the *ab* plane with their BTK fittings (thin lines). Two separate sets of gap minima are clearly seen at low fields.

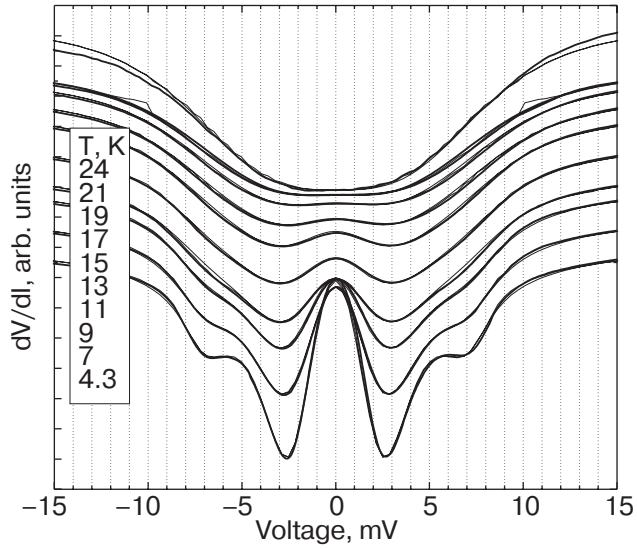

Fig. 13. Temperature dependences of dV/dI curves (solid lines) for the same junction as in Fig. 12 with their BTK fittings (thin lines).

observation of dV/dI-gap structure in Fig. 11 with visually only the larger gap present. This gap persists in a magnetic field of a few tesla, unlike the smaller gap, which according to [43,44], vanishes above 1 T. Spectra of that kind were not observed in thin films. This means that the conductivity is governed only by the σ band. This may be caused by the circumstance that the π band is blocked completely by Mg disorder or by oxidation of Mg atoms on *ab* side surface of the crystal. At the same time, in a single crystal there is much less scattering in the boron planes, due to the robustness of the B – B bonds. We will see below that just this case

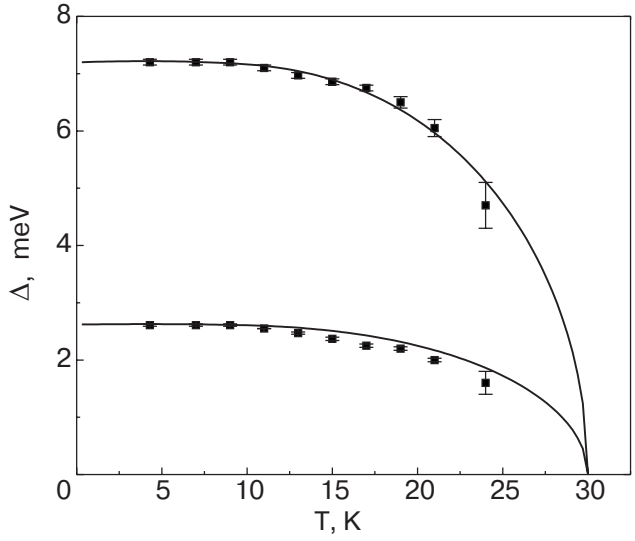

Fig. 14. Temperature dependences of large and small superconducting energy gaps obtained by BTK fitting from Fig. 13. The solid lines represent BCS-like behavior.

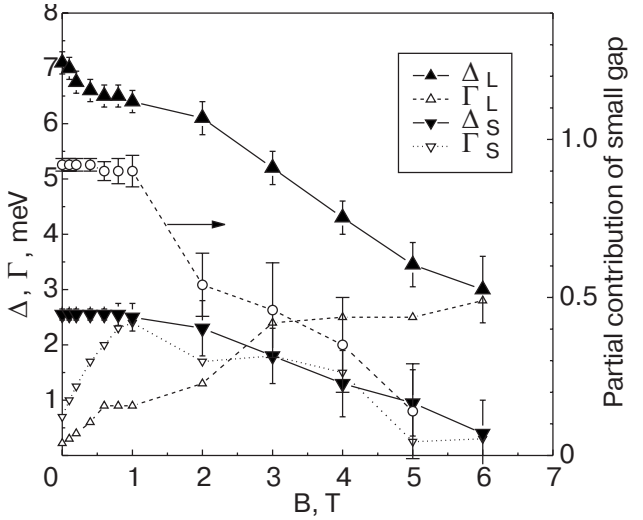

Fig. 15. Magnetic field dependences of the large and small superconducting energy gaps (solid triangles) obtained by BTK fitting from Fig. 12. Open triangles show the Γ value for large and small gap, respectively. The circles demonstrate the depression of the small-gap contribution to the dV/dI spectra by magnetic field. The lines connect the symbols for clarity.

enables us to observe directly the most important E_{2g} phonon mode in the electron–phonon interaction within the σ band.

In single crystals the negative slope in dV/dI curve at large biases is observed quite often, which confirms that the disorder in the π band leads to quasi-localization of charge carriers. An example of this is already shown in Fig. 10.

Figures 12 and 13 display a series of magnetic-field and temperature dependence of dV/dI curves with their BTK fittings. Here the two gaps are clearly visible, corresponding to the theoretical prediction, in the *ab* direction Eq. (11). The temperature dependence of both gaps follows the BCS prediction (see Fig. 14). For temperatures above 25 K their behavior is unknown because this particular contact did not survive the measurements, likely due to thermal expansion of the sample holder.

Figure 15 displays the magnetic-field dependences of large and small gaps. Surprisingly, the small gap value is not much depressed by a field of about 1 T, and the estimated critical field about 6 T is much higher, as stated in [44,45], although the intensity of the small-gap minima is suppressed rapidly by a field of about 1 T. Correspondingly, the small-gap contribution w* to the dV/dI spectra is decreased by magnetic field significantly, from 0.92 to 0.16 (see

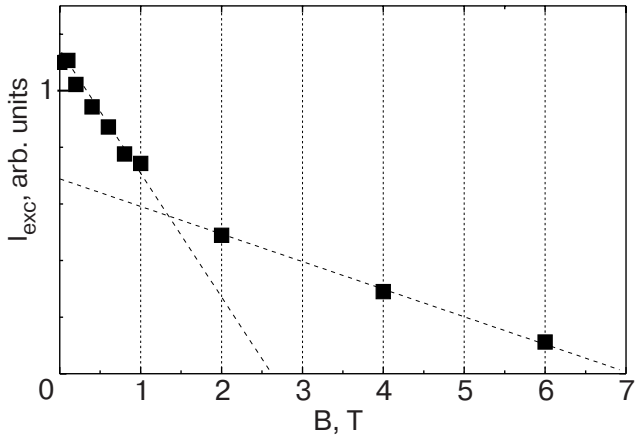

Fig. 16. $I_{exc}(B)$ (squares) for a MgB_2–Cu junction from Fig. 12. The dashed lines show the different behavior of $I_{exc}(B)$ at low and high fields.

Fig. 15), while w versus temperature even increases slightly from 0.92 at 4.3 K to 0.96 at 24 K (not shown).

The area under the energy-gap minima in $dV/dI(V)$ is approximately proportional to the excess current I_{exc} (see Eq. (4)) at $eV >> \Delta$ (or roughly to the superfluid density). The excess current depends on the magnetic field with a positive overall curvature (Fig. 16). $I_{exc}(B)$ decreases abruptly at first and then more slowly above 1 T. This corresponds to a drastic depressing of the $dV/dI(V)$ small-gap-minima intensity by a magnetic field of about 1 T and to robustness

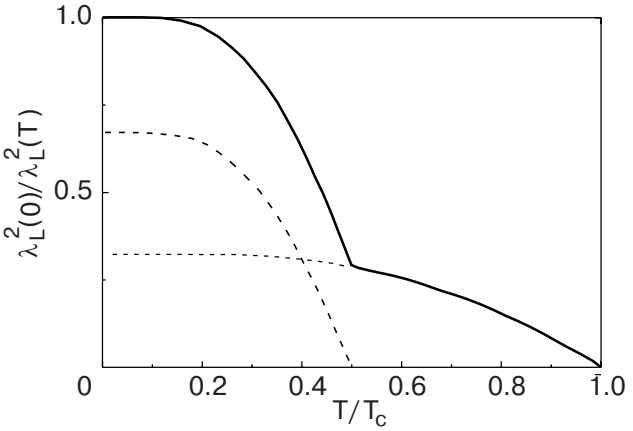

Fig. 17. Temperature dependence of the penetration depth in the model of two independent BCS superconducting bands (dashed and dotted line) with different superconducting gaps. The resulting penetration depth (solid line) clearly shows a non-BCS temperature behavior. The low-temperature behavior will be dominated by the band with the smaller superconducting gap. After Golubov et al. [46].

* w inversely depends on Γ value, therefore nearly constant w value between 0 and 1 T is due to the fact that Γ rises by factor 4 at 1 T.

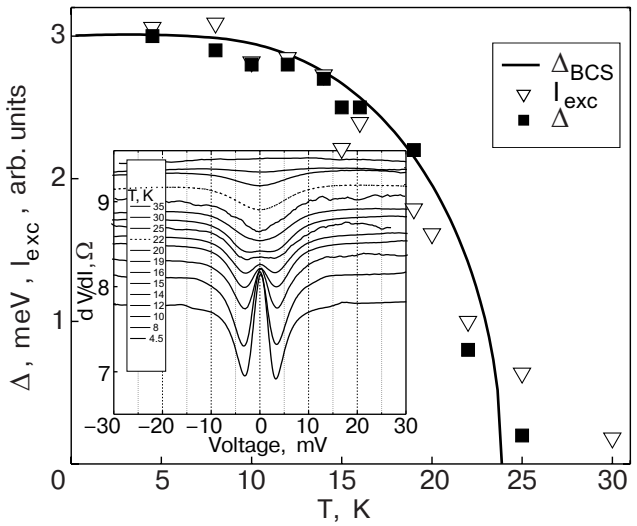

Fig. 18. Temperature dependence of a single superconducting energy gap (squares) obtained by BTK fitting of dV/dI curves from inset. The solid lines represent BCS-like behavior. The triangles show the dependence of the excess current. Inset: dV/dI curves for a MgB_2-Cu 8 Ω contact at different temperatures.

of the residual superconducting structure against further increase of magnetic field. This is a quite different dependence from what is expected for I_{exc}, which is in general proportional to the gap value (4).

In contrast, $I_{exc}(T)$ has mostly negative curvature and shape, similar to the BCS dependence. Often a positive curvature appears above 25 K (see e.g. Fig. 18).

This kind of anomaly can be due to the two-band nature of superconductivity in MgB_2, since the magnetic field (temperature) suppresses the superconductivity more quickly in the π band and then, at higher field (temperature), in the σ band. The same consideration is valid for $1/\lambda_L$, which is roughly proportional to the «charge density of superfluid condensate». In the case of zero interband scattering, the simple model [46] predicts the temperature dependence shown in Fig. 17 for σ and π parallel channels, which will yield a smooth curve with general positive curvature, taking into account the small interband scattering occurring in reality.

If the π-band conductivity is blocked by a short mean free path, then the curvature of $I_{exc}(T)$, being proportional to $\Delta_\sigma(T)$, should be negative, which supplies us with additional confirmation of single-band conductivity along the σ band. Thus, measuring the magnetic field and temperature dependences of I_{exc} can elucidate the contact structure.

Figure 18 displays the temperature dependence of the gap for the dV/dI curves with a single-gap structure, which vanishes around 25 K. A magnetic field of 1 T suppresses the gap minima intensity by factor of

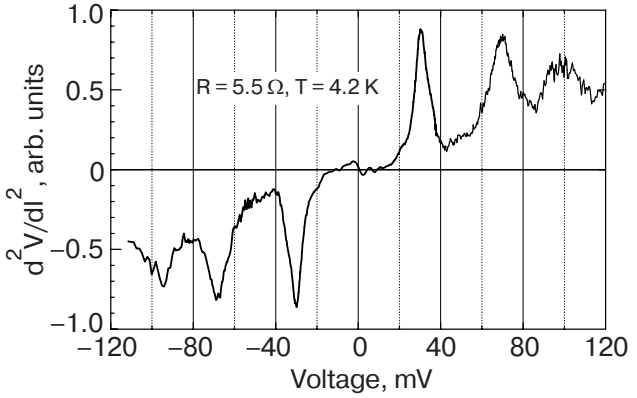

Fig. 19. Raw PC EPI spectrum for a ZrB_2 5.5 Ω point contact at 4.2 K. After Naidyuk et al. [47].

two, but the minima are clearly seen even at 4 T (not shown), the maximal field in this experimental trial. This excludes an origin of these gap minima due to a small gap. According to the calculation in [11] a large amount of impurity scattering will cause the gaps to converge to $\Delta \simeq 4.1$ meV and T_c to 25.4 K. Therefore these single-gap spectra reflect a strong interband scattering due to impurities, which likely causes a «semiconducting-like» behavior of dV/dI above T_c (see Fig. 18, inset). $I_{exc}(T)$ behaves nearly as $\Delta(T)$ except in the region $T > 25$ K, where I_{exc} is still nonzero because of a residual shallow zero-bias minimum in dV/dI above 25 K.

4.2. Phonon structure in the $I-V$ characteristics

PC EPI spectra of nonsuperconducting diborides. We have studied the PC EPI spectra $d^2V/dI^2 \propto -d^2I/dV^2$ (see also Eq. (3)) of non-

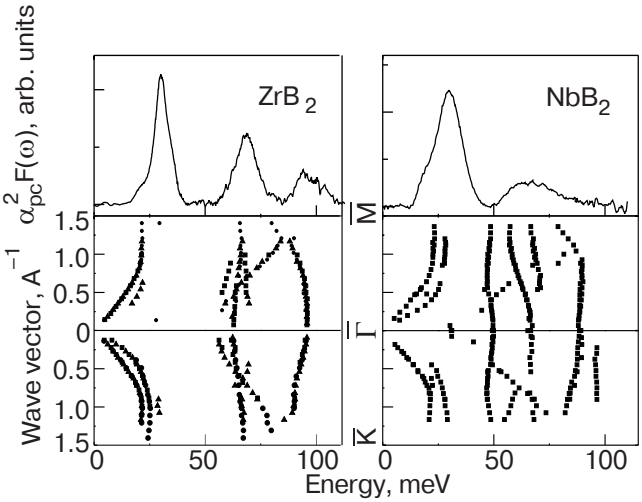

Fig. 20. Comparison of high-resolution electron-energy-loss spectroscopy measurements of surface phonon dispersion (bottom panels, symbols) [49] with the PC spectra for ZrB_2 and NbB_2 after subtraction of the rising background (upper panels).

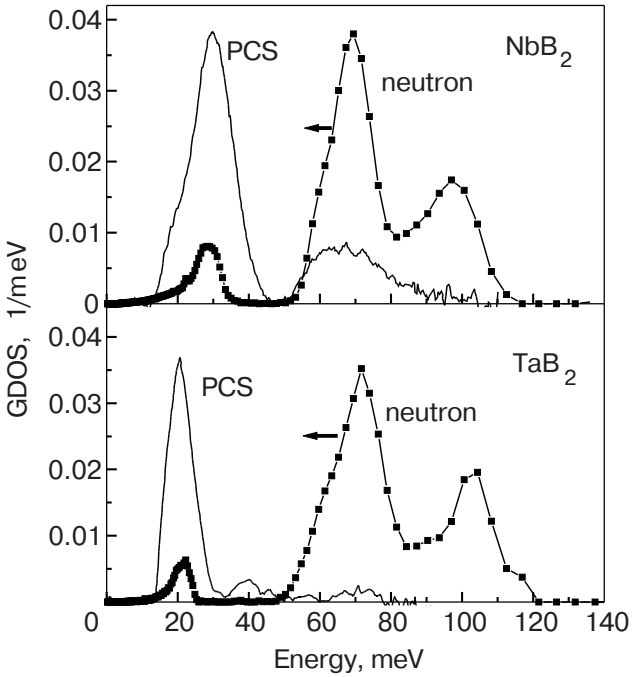

Fig. 21. Comparison of phonon DOS neutron measurements after Heid et al. [48] (symbols) with PC spectra for TaB_2 and NbB_2 after subtraction of the rising background (solid curves).

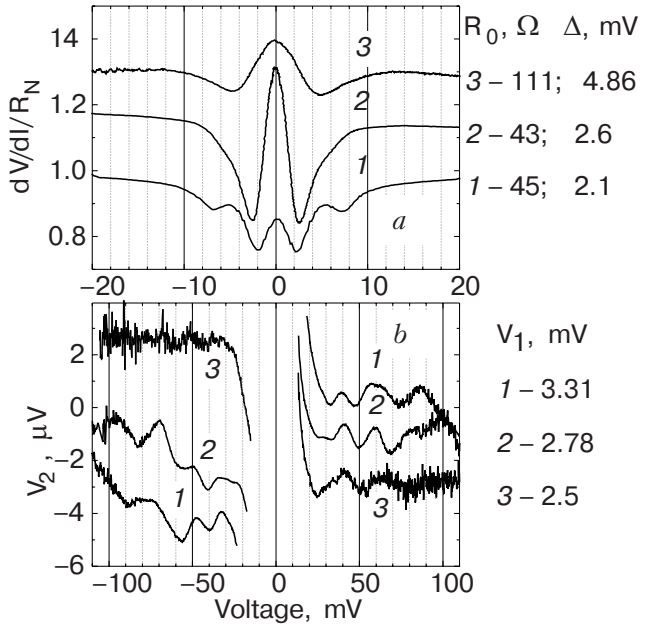

Fig. 23. Superconducting gap features (upper panel) and phonon structure (bottom panel) in the spectra of thin-film MgB_2-Ag junctions with different resistances at $T = 4.2$ K, $B = 0$. After Yanson et al. [23].

superconducting diborides MeB_2 (Me = Zr, Nb, Ta) [47]. The cleanest sample we have is a ZrB_2 single crystal, and its PC EPI spectrum is shown in Fig. 19. One recognizes a classical PC EPI spectrum from which one can estimate the position of 3 main phonon peaks and obtain the lower limit of EPI parameter λ_{PC} [47].

Essentially similar spectra were observed for other diborides, taking into account their purity and increased EPI, which leads to a transition from the spectroscopic to a non-spectroscopic (thermal) regime of current flow [47]. The positions of the low-energy peaks are proportional to the inverse square root of the masses of the *d* metals [47], as expected. For these compounds the phonon density of states is measured by means of neutron scattering [48] and the surface phonon dispersion is derived by high-resolution electron-energy-loss spectroscopy [49]. The positions of the phonon peaks or $d\omega/dq = 0$ for the dispersion curves correspond to maxima of the PC spectra (Fig. 20, Fig. 21).

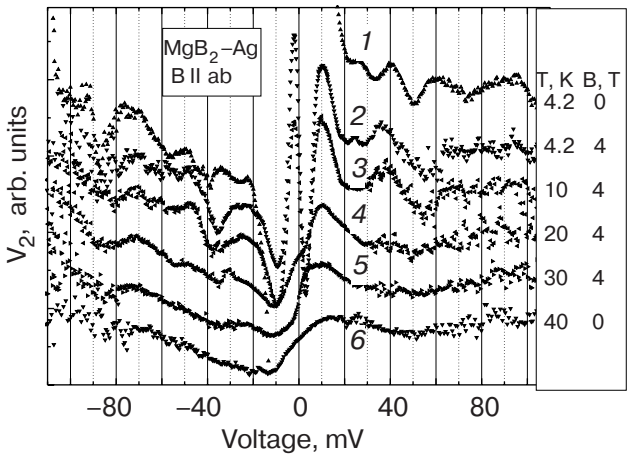

Fig. 22. Phonon singularities in the PC spectra of a MgB_2 thin-film – Ag junction as a function of magnetic field and temperature. T and B are shown beside each curve. After Yanson et al. [23].

PC EPI spectra of MgB_2 *in c-axis oriented films.* From the above considerations we had anticipated that one could easily measure the EPI spectral function of MgB_2 in the normal state, provided that the superconductivity is destroyed by magnetic field. Unfortunately, that was not the case. The stronger we suppress the superconductivity in MgB_2, the less traces of phonon structure remain in the $I-V$ characteristic and its derivatives (Fig. 22) [23]. This is in odd in relation to the classical PCS, since the *inelastic* phonon spectrum should not depend on the state of electrodes in the first approximation (see Sec. Theoretical background).

Instead, most of the MgB_2 spectra in the superconducting state show reproducible structure in the phonon energy range (Fig. 23) which was not similar to the expected phonon maxima superimposed on the rising background. This structure disappears upon transition to the normal state. Quite interestingly the

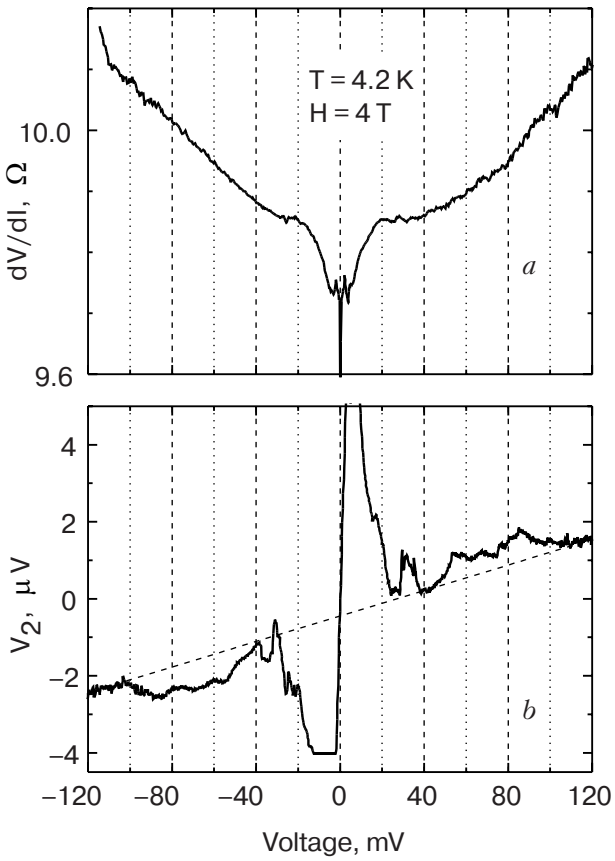

Fig. 24. dV/dI and $V_2 \propto d^2V/dI^2$ curves for a thin-film MgB_2—Ag junction revealing the inelastic PC spectrum for the π band. After Bobrov et al. [50].

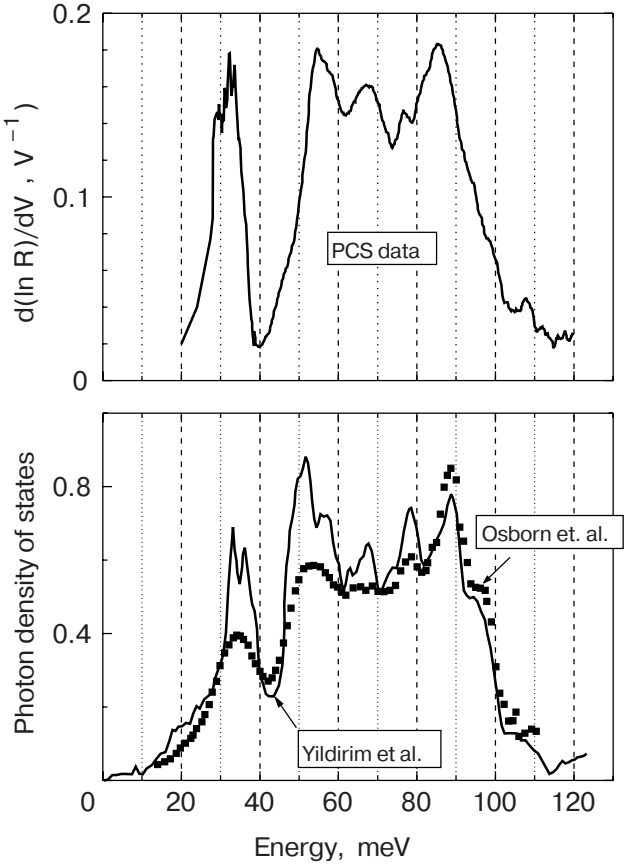

Fig. 25. Comparison of the PC EPI spectrum (upper panel) from Fig. 24 (after subtraction of the linear background and zero-bias maxima below 25 meV) with the phonon DOS measured by neutron scattering [8,13] (bottom panel).

intensity of this structure increases with increase of the value of the small gap, which means that the gap in the π band and observed phonon structure is connected [23]. Based on the theoretical consideration mentioned in the Introduction, we conclude that the disorder in the π band is so strong that it precludes observation of the *inelastic current*, and the phonon nonlinearities of the excess current (see Eq. (6)) play the main role, which does not depend on the scattering.

Very rarely we did see signs that the observed characteristics indeed satisfy the conditions imposed on the inelastic PC spectra. One such example is shown in Figs. 24, 25. For this particular junction the superconducting peculiarities are almost completely suppressed above 20 mV in moderate field (4 T). What remains is a very weak structure (~1 %) from the rather high value of the gap (Fig. 24). The background in $dV/dI(V)$ rises nearly quadratically up to a few % of R_0 at large biases (~ 100 mV). This leads to a linear background in $V_2 \propto d^2V/dI^2(V)$ with phonon peaks superposed above the background both in negative and positive bias polarity (compare with Fig. 19). The structure observed corresponds reasonably in shape above 30 meV to the phonon density of states (Fig. 25). At low voltages (below 30 meV), most probable, the gap peculiarities still prevail over $d^2V/dI^2(V)$ structure. Thus, for this contact we assume to observe the *inelastic* PC spectrum for the π band, which should be compared to the Eliashberg EPI function for the same band calculated in Ref. 51

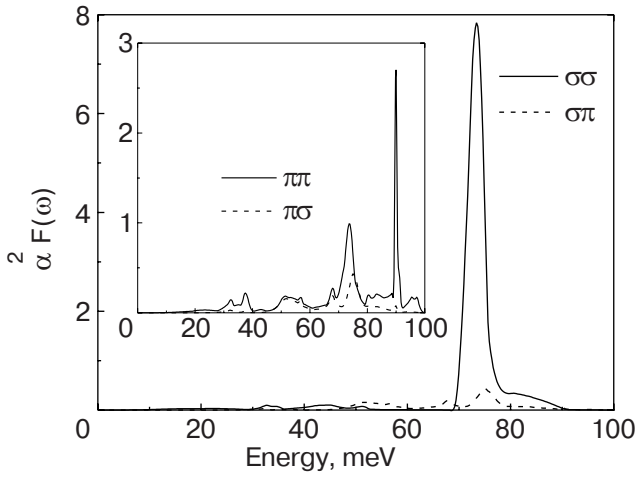

Fig. 26. Calculated Eliashberg functions for the σ and π bands (inset). After Golubov et al. [51].

(Fig. 26). Both the experimental spectrum and the π-band Eliashberg function do not show anomalously high intensity of the E_{2g} phonon mode, since only the Eliashberg function for σ band is the principal driving force for high T_c in MgB_2. The same conclusion should be ascribed to the excess-current phonon structure, since it also corresponds to the π band. This band has much larger Fermi velocity and plasma frequency along the *c* axis compared to the σ band [11].

Thus, in order to register the principal EPI with the E_{2g} phonon mode, we are faced with the necessity of measuring the PC spectra for only the σ band. This can be done in a single crystal along the *ab* plane with blocked π-band conductivity.

PC EPI spectra of MgB_2 *in the ab direction*. The desired situation was described in Ref. 52 for a single crystal oriented in the *ab* plane. As was mentioned above, the nominal orientation of the contact axis to be parallel to *ab* plane is not enough to be sure that this situation occurs in reality. Moreover, even if one establishes the necessary orientation (i.e., contact axis parallel to *ab* plane) the spectra should reflect both bands with a prevalence of the undesired π band, because due to spherical spreading of the current the orientational selectivity of a metallic point contact is much worse than that for the plane tunnel junction, where it goes exponentially. The large mixture of π-band contribution is clearly seen from the gap structure in Fig. 27. Beyond the wings at the biases corresponding to the large gap (supposed to belong to the σ-band gap) the deep minima located at the smaller gap (correspondingly to the π-band gap) are clearly seen (see bottom panel of Fig. 27). The EPI spectrum of the same junction is shown in the upper panel. One can see that the nonlinearities of the $I-V$ characteristic at phonon biases are very small, and a reproducible structure roughly corresponding to the Eliashberg EPI function of the π band [38,51] appears in the bias range ~ 20–60 mV. Above 60 mV the PC spectrum broadens sufficiently hidden higher-lying phonon maxima.

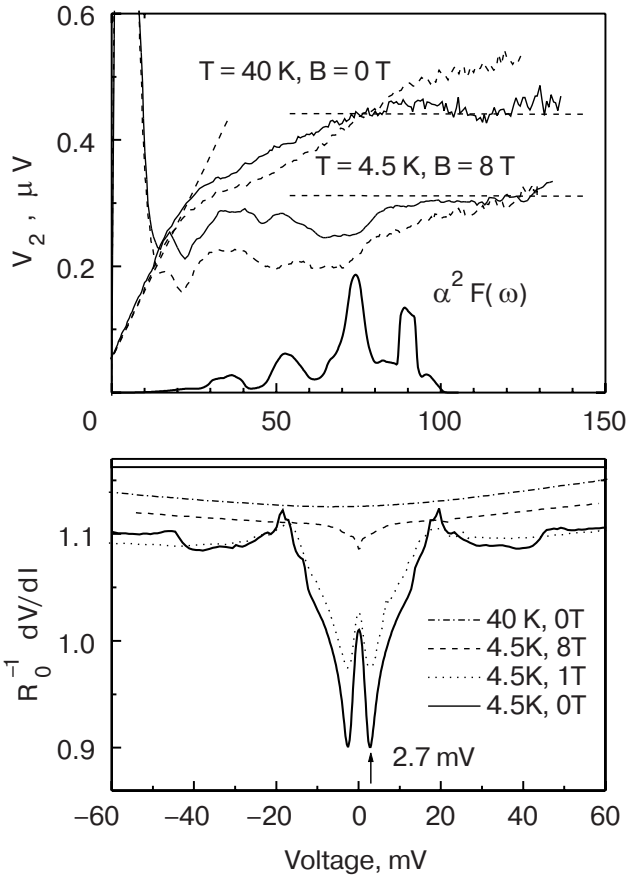

Fig. 27. $V_2 \propto d^2V/dI^2$ (for two bias voltage polarities) and dV/dI curves for a single-crystal MgB_2-Cu junction ($R_0 = 1.5\ \Omega$) along the *ab* plane. Here the conductivity along the π band prevails, as is shown by the pronounced small-gap structure for the zero-field dV/dI curve at 4.5 K. The $\alpha^2F(\omega)$ curve is the theoretical prediction for the π-band Eliashberg function from Fig. 26 (inset) smeared similarly to the experimental data. After Naidyuk et al. [52].

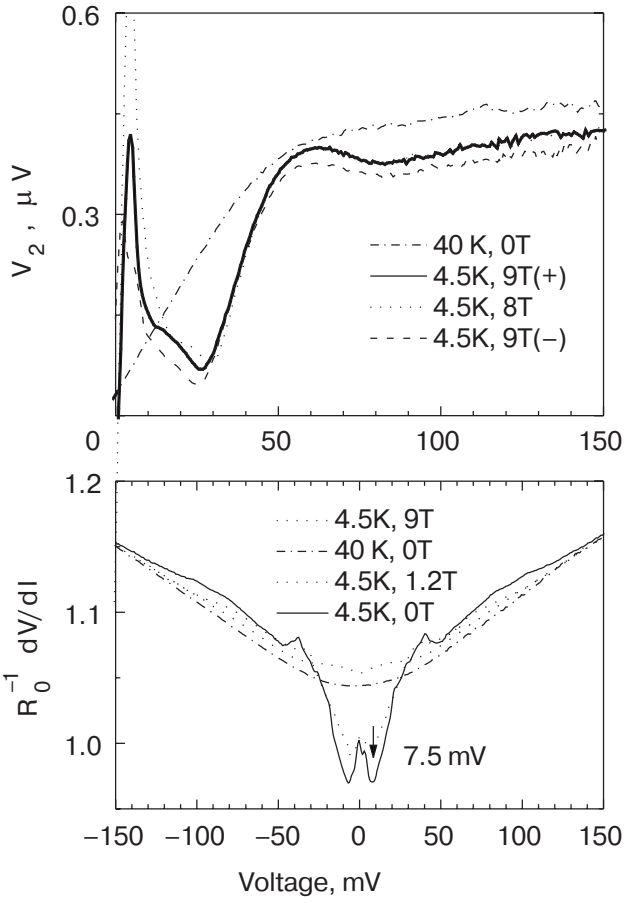

Fig. 28. $V_2 \propto d^2V/dI^2$ (for two bias voltage polarities at 9 T) and dV/dI curves for a single-crystal MgB_2-Cu junction ($R_0 = 7.2\ \Omega$) along the *ab* plane. Here the conductivity along the σ band prevails, as is shown by the pronounced large-gap structure for the zero-field dV/dI-curve at 4.5 K. After Naidyuk et al. [52].

Even in the normal state ($T \geq T_c$), where the excess current disappears, one can see the kink at ≈ 20–30 meV, where the first peak of the phonon DOS and the first maximum of the Eliashberg EPI function of the π band occurs. At $eV \approx 90$–100 meV the PC EPI spectrum of Fig. 27 saturates just where the phonon DOS ends. At $T \geq T_c$ intermediate phonon peaks are hardly seen, since the thermal resolution, which equals $5.44k_BT$, amounts about 20 meV, and the regime of current flow is far from ballistic, due to the high background observed. No prevalence of the E_{2g} phonon mode is observed, like a big maximum of EPI at ≈ 60–70 meV or a kink at $T \geq T_c$ for these biases.

A quite different spectrum is shown in Fig. 28, which is our key result. Consider first the $dV/dI(V)$ characteristics (see bottom panel). The energy gap structure shows the gap minima corresponding to the large gap (σ-band gap). The increase of $dV/dI(V)$ at larger biases is noticeably larger than in the previous case (Fig. 27). One can notice that the relatively small magnetic field (~1 T) does not decrease the intensity of gap structure substantially, unlike those for Fig. 12, and even less than for Fig. 27. According to [43,44] a field of about 1 T should depress the small-gap intensity completely.

All these facts evidence that we obtain a contact in which only the σ-band channel in conductivity is operated.

Let us turn to the PC EPI spectra $d^2V/dI^2(V)$, which are connected via the following expression to the second harmonic signal V_2 recorded in experiment:

$$\frac{1}{R^2}\frac{d^2V}{dI^2} = 2\sqrt{2}\,\frac{V_2}{V_1^2}\ .$$

Here $R = dV/dI$ and V_1 is the rms value of the modulation voltage for the standard techniques of tunneling and point-contact spectroscopy.

The PC EPI spectra for this contact are shown in Fig. 28 (upper panel) for the highest field attainable in our experiments [52]. One can see that 8–9 T is still not enough to destroy completely the superconductivity in the energy-gap low bias range (0–30 meV), which can be taken as characteristic for a strongly superconducting σ band. On the other hand, at larger biases no influence of field is noted, which evidences that this part of I–V characteristic does not contains superconducting peculiarities, likely due to the high current density in the contact. Except for a small asymmetry, the spectrum is reproduced for both polarities. Before saturation at biases ≥ 100 meV, where the phonon DOS ends, a well-resolved wide bump occurs, which is located at about 60 meV. Further on, we will concentrate on this.

First, we rescale it to the spectrum in $R_0^{-1}dR/dV$ units, in order to compare with the theoretical estimation. We will show that the bump is of spectroscopic

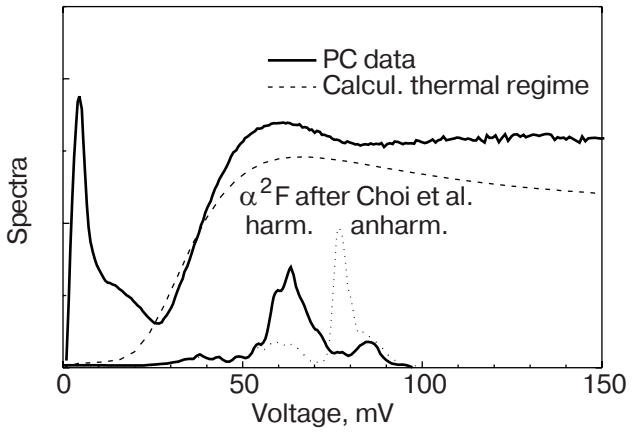

Fig. 29. Comparison of the experimental spectrum of Fig. 28 with the thermal spectrum for a model spectral function in the form of a Lorentzian at 60 meV with a width of 2 meV (dashed line) and with the theoretical EPI spectra (bottom curves). After Naidyuk et al. [52].

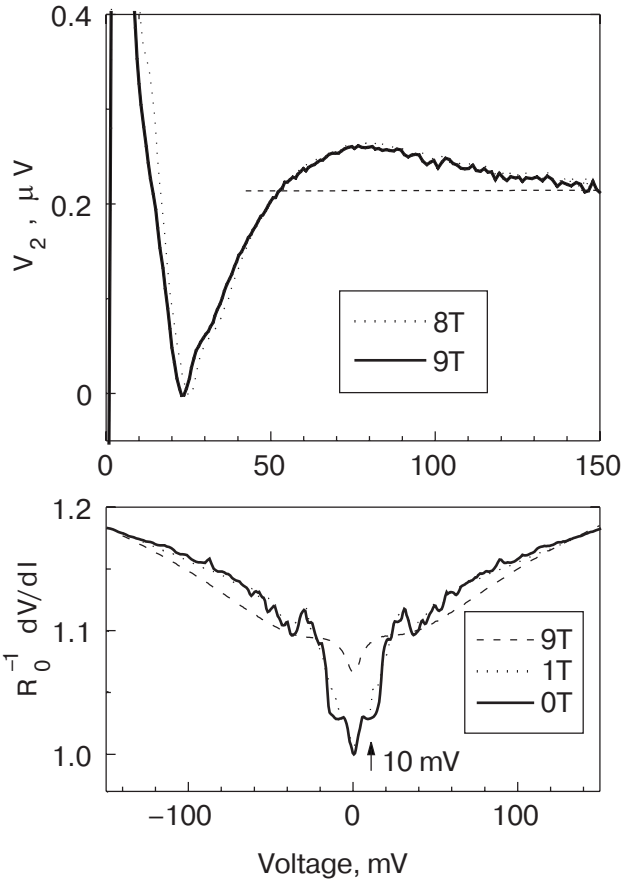

Fig. 30. Thermal limit for the σ band (as is shown by the pronounced large-gap structure for the zero-field dV/dI curve at 4.5 K) in the PC spectrum of a MgB_2 single crystal along the *ab* plane. After Naidyuk et al. [52].

origin, i.e., the regime of current flow through the contact is not thermal, although the background at large biases ($V \geq 100$ meV) is high. To do so, we compare this bump with a PC spectrum in the thermal regime for a model EPI function, which consists of a Lorentzian at 60 meV with small (2 meV) width. Calculated according to Kulik [53], the thermal PC EPI spectrum is much broader, shown in Fig. 29 as a dashed line. Any further increase of the width of the model spectra will broaden the curve obtained. Comparing the experimental and model spectra enable us to conclude that, in spite of the large width, the maximum of the experimental spectra still corresponds to the spectroscopic regime. The high-temperature ($T \geq T_c$) spectrum in Fig. 28 shows the smeared kink at about 60 meV, unlike that of Fig. 27. Introducing greater disorder in the boron plane by a fabrication procedure or by trying other spots on the side-face surface, the smeared thermal spectra were observed, coinciding in shape with the dashed curve in Fig. 30. In this figure another junction is shown, where the energy gap structure also points to the σ-band channel. Other junctions display the kink at about 30–40 meV, like the high-temperature spectrum in Fig. 27, which together with their energy-gap structure can be ascribed to the thermal limit mainly in the π band, despite the rather low bath temperature.

A PC spectrum with broad maxima including one at about 60 mV was observed in [45] on polycrystalline MgB_2 samples driven to the normal state by applying moderate magnetic field and increasing the temperature.

The large width of the EPI peak connected with the E_{2g} phonon mode (Fig. 28) is not surprising. Shukla et al. [14] measured the phonon dispersion curves along the ΓA and ΓM directions by means of inelastic x-ray scattering (see Fig. 4). The full width at half maximum for the E_{2g} mode along the ΓA direction amounts about 20–28 meV, which corresponds well to what we observe in the point-contact spectrum. If the phonon lifetime corresponds to this (inverse) energy, then the phonon mean free path is about equal to the lattice constant [52], and due to phonon reabsorption by accelerating electrons, we should anticipate a large background in the PC spectra as observed. If we compare the position of the bump (≈ 60 meV) with what is predicted for isotropic Eliashberg EPI function [19] (see Fig. 29), then we, together with Shukla et al., should admit that the phonon–phonon anharmonicity is inessential for this mode, and its high width is due completely to the EPI.

Now turn to the nonlinearity of the $I-V$ curves due to the electron–phonon interaction, which can be estimated from the dV/dI curves as about 10% for contact with the E_{2g} phonon modes in Fig. 28. This is comparable with the nonlinearity observed for nonsuperconducting diborides [47] with a small electron–phonon coupling constant. The reason for the relatively low nonlinearity of the $I-V$ curves and low intensity of the principal E_{2g} phonon modes in the spectra for the MgB_2 contacts can be the fact that anomalous strong interaction is characteristic for restricted group of phonons with sufficiently small wave vector [9], whereas in point-contact spectroscopy the large-angle scattering is underlined.

5. Conclusions

We made an overview of the PCS investigations of *c*-axis oriented thin films and single crystals of MgB_2. Our conclusions are as follows:

1. There are two different superconducting gaps in MgB_2, which are grouped at 2.4 and 7.0 meV. Roughly, in half of all point contacts studied for *c*-axis oriented films the two gap structure merges together due to strong elastic scattering remaining a single gap at about 3.5 meV.

2. Anomalous temperature and especially magnetic field dependences of excess current in point-contact junctions reflect the two-band structure of the superconducting order parameter in MgB_2.

3. There are two mechanisms of revealing phonon structure in the point-contact spectra of MgB_2: i) through the inelastic backscattering current, like for ordinary point-contact spectroscopy, and ii) through the energy dependence of the excess current, like in the similar tunneling spectroscopy of the electron–phonon interaction. They can be discriminated by destroying the superconductivity with a magnetic field and/or temperature and by varying the electron mean free path.

4. The prevailing appearance of the E_{2g} boron mode, which mediates the creation of Cooper pairs, is seen in the PC spectra only along the *a*–*b* direction in accordance with the theory. The relatively small intensity of this mode in the PC spectra is likely due to their small wave vector and restricted phase volume.

5. Related diborides (ZrB_2, NbB_2, and TaB_2) have d^2V/dI^2 spectra proportional to the electron–phonon interaction spectral function like that in common metals and a small EPI constant corresponding to their nonsuperconducting state.

Acknowledgements

The authors are grateful to N.L. Bobrov, P.N. Chubov, V.V. Fisun, O.E. Kvitnitskaya, L.V. Tyutrina for collaboration during the MgB_2 investigation. IKY thanks the Institute of Solid State Physics in For-

schungzentrum Karlsruhe for hospitality, and Prof. H. von Löhneysen for constant support. The work in Ukraine was supported by the State Foundation of Fundamental Research under Grant F7/528-2001.

Note added in proof

After the paper was completed we have learned of the paper by Koshelev and Golubov [54], where the magnetic field dependence of Δ_σ and Δ_π was presented. It turned out that the $\Delta_\sigma(B)$ and $\Delta_\pi(B)$ behavior is different and is governed by diffusion constants depending on the coherence length. However, the critical field is the same both for Δ_σ and Δ_π. This is in line with our observation given in Fig. 15. Additionally, two experimental reports on the effect of magnetic field on both gaps in MgB_2 by Gonnelli et al. (cond-mat/0308152) and Bugoslavsky et al. (cond-mat/0307540) appeared in the E-print archive. Bugoslavsky et al. reported that both order parameters persist to a common magnetic field. Gonnelli et al. corrected their previous claims and mentioned that identification of the magnetic field at which the π-band features in dV/dI visually disappear with the critical field for the π band might not be correct.

1. Jun Nagamatsu, Norimasa Nakagawa, Takahiro Muranaka, Yuji Zenitani, and Jun Akimitsu, *Nature* **410**, 63 (2001).
2. I.I. Mazin, O.K. Andersen, O. Jepsen, O.V. Dolgov, J. Kortus, A.A. Golubov, A.B. Kuz'menko, and D. van der Marel, *Phys. Rev. Lett*. **89**, 107002 (2002).
3. A. Gurevich, *Phys. Rev*. **B67**, 184514 (2003*)*.
4. J.M. An and W.E. Pickett, *Phys. Rev. Lett*. **86**, 4366 (2001).
5. Y. Kong, O.V. Dolgov, O. Jepsen, and O.K. Andersen, *Phys. Rev*. **B64**, 020501(R) (2001).
6. J. Kortus, I.I. Mazin, K.D. Belashchenko, V.P. Antropov, and L.L. Boyer, *Phys. Rev. Lett*. **86**, 4656 (2001).
7. Amy Y. Liu, I.I. Mazin, and Jens Kortus, *Phys. Rev. Lett.* **87**, 087005 (2001).
8. T. Yildirim, O. Gülseren, J.W. Lynn, C.M. Brown, T.J. Udovic, Q. Huang, N. Rogado, K.A. Regan, M.A. Hayward, J.S. Slusky, T. He, M.K. Haas, P. Khalifah, K. Inumaru, and R.J. Cava, *Phys. Rev. Lett*. **87**, 037001 (2001).
9. I.I. Mazin and V.P. Antropov, *Physica* **C385**, 49 (2003).
10. Yu. Eltsev, K. Nakao, S. Lee, T. Masui, N. Chikumoto, S. Tajima, N. Koshizuka, and M. Murakami, *Phys. Rev*. **B66**, 180504(R) (2002).
11. A. Brinkman, A.A. Golubov, H. Rogalla, O.V. Dolgov, J. Kortus, Y. Kong, O. Jepsen, and O.K. Andersen, *Phys. Rev.* **B65**, 180517 (2002).
12. V.G. Kogan and S.L. Bud'ko, *Physica* **C385**, 131 (2003).
13. R. Osborn, E.A. Goremychkin, A.I. Kolesnikov, and D.G. Hinks, *Phys. Rev. Lett*. **87**, 017005 (2001).
14. Abhay Shukla, Matteo Calandra, Matteo d'Astuto, Michele Lazzeri, Francesco Mauri, Christophe Bellin, Michael Krisch, J. Karpinski, S.M. Kazakov, J. Jun, D. Daghero, and K. Parlinski, *Phys. Rev. Lett.* **90**, 095506 (2003).
15. K.-P. Bohnen, R. Heid, and B. Renker, *Phys. Rev. Lett.* **86**, 5771 (2001).
16. James William Quilty, *Physica* **C385**, 264 (2003).
17. A.F. Goncharov and V.V. Struzhkin, *Physica* **C385**, 117 (2003).
18. Hyoung Joon Choi, David Roundy, Hong Sun, Marvin L. Cohen, and Steven G. Louie, *Nature* **418**, 758 (2002).
19. Hyoung Joon Choi, David Roundy, Hong Sun, Marvin L. Cohen, and Steven G. Louie, *Phys. Rev.* **B66**, 020513(R) (2002).
20. J.M. An, S.Y. Savrasov, H. Rosner, and W.E. Pickett, *Phys. Rev*. **B66**, 220502(R) (2002).
21. E. Cappelluti, S. Ciuchi, C. Grimaldi, L. Pietronero, and S. Strässler, *Phys. Rev. Lett*. **88**, 117003 (2002).
22. F. Bouquet, Y. Wang, I. Sheikin, P. Toulemonde, M. Eisterer, H.W. Weber, S. Lee, S. Tajima, and A. Junod, *Physica* **C385**, 192 (2003).
23. I.K. Yanson, V.V. Fisun, N.L. Bobrov, Yu.G. Naidyuk, W.N. Kang, Eun-Mi Choi, Hyun-Jung Kim, and Sung-Ik Lee, *Phys. Rev*. **B67**, 024517 (2003).
24. W.N. Kang, Hyeong-Jin Kim, Eun-Mi Choi, C.U. Jung, and Sung-Ik Lee, *Science* **292**, 1521 (2001).
25. W.N. Kang, Eun-Mi Choi, Hyeong-Jin Kim, Hyun-Jung Kim, and Sung-Ik Lee, *Physica* **C385**, 24 (2003).
26. Sergey Lee, *Physica* **C385**, 31 (2003); S. Lee, H. Mori, T. Masui, Yu. Eltsev, A. Yamanoto and S. Tajima, *J. Phys. Soc. Jpn*. **70**, 2255 (2001).
27. J.W. Quilty, S. Lee, A. Yamamoto, and S. Tajima, *Phys. Rev. Lett*. **88**, 087001(2001).
28. J.M. Rowell, *Supercond. Sci. Technol.* **16**, R17 (2003).
29. V.A. Khlus and A.N. Omel'yanchuk, *Fiz. Nizk. Temp.* **9**, 373 (1983) [*Sov. J. Low Temp. Phys*. **9**, 189 (1983)].
30. V.A. Khlus, *Fiz. Nizk. Temp.* **9**, 985 (1983) [*Sov. J. Low Temp. Phys.* **9**, 510 (1983)].
31. I.O. Kulik, A.N. Omelyanchouk, and R.I. Shekhter, *Fiz. Nizk. Temp.* **5**, 1543 (1977) [*Sov. J. Low Temp. Phys*. **3,** 840 (1977)].
32. I.K. Yanson, in: *Quantum Mesoscopic Phenomena and Mesoscopic Devices in Microelectronic*, I.O. Kulik and R. Ellialtioglu (eds.), (2000) p. 61, Kluwer Academic Publishers (see also: *cond-mat/0008116*).
33. A.N. Omel'yanchuk, S.I. Beloborod'ko, and I.O. Kulik, *Fiz. Nizk. Temp.* **17**, 1142 (1988) [*Sov. J. Low Temp. Phys*. **14**, 630 (1988)].
34. S.I. Beloborod'ko and A.N. Omel'yanchuk, *Fiz. Nizk. Temp.* **17**, 994 (1991) [*Sov. J. Low Temp. Phys*. **17**, 518 (1991)].
35. S.I. Beloborod'ko, private communicatrion.

36. E.L. Wolf, *Principles of Electron Tunneling Spectroscopy*, Oxford University Press, London (1985).
37. R.D. Parks, *Superconductivity*, Marcel Dekker Inc., New York (1969).
38. O.V. Dolgov, R.S. Gonnelli, G.A. Ummarino, A.A. Golubov, S.V. Shulga, and J. Kortus, *Phys. Rev.* **B68**, 132503 (2003).
39. G.E. Blonder, M. Tinkham, and T.M. Klapwijk, *Phys. Rev.* **B25**, 4515 (1982).
40. Yu.G. Naidyuk, I.K. Yanson, L.V. Tyutrina, N.L. Bobrov, P.N. Chubov, W.N. Kang, Hyeong-Jin Kim, Eun-Mi Choi, and Sung-Ik Lee, *JETP Lett.* **75**, 283 (2002).
41. A.B. Kuz'menko, F.P. Mena, H.J.A. Molegraaf, D. van der Marel, B. Gorshunov, M. Dressel, I.I. Mazin, J. Kortus, O.V. Dolgov, T. Muranaka, and J. Akimitsu, *Solid State Commun.* **121**, 479 (2002).
42. I.I. Mazin, O.K. Andersen, O. Jepsen, A.A. Golubov, O.V. Dolgov, and J. Kortus, *Phys. Rev.* **B69**, 056501 (2004).
43. P. Szabó, P. Samuely, J. Kacmarćik, Th. Klein, J. Marcus, D. Furchart, S. Miragila, C. Marcenat, and A.G.M. Jansen, *Phys. Rev. Lett.* **87** 137005 (2001).
44. R.S. Gonnelli, D. Daghero, G.A. Ummarino, V.A. Stepanov, J. Jun, S.M. Kazakov, and J. Karpinski, *Phys. Rev. Lett.* **89**, 247004 (2002).
45. P. Samuely, P. Szabó, J. Kacmarćik, T. Klein, and A.G.M. Jansen, *Physica* **C385**, 244 (2003).
46. A.A. Golubov, A. Brinkman, O.V. Dolgov, J. Kortus, and O. Jepsen, *Phys. Rev*. **B66**, 054524 (2002).
47. Yu.G. Naidyuk, O.E. Kvitnitskaya, I.K. Yanson, S.-L. Drechsler, G. Behr, and S. Otani, *Phys. Rev.* **B66**, 140301 (2002).
48. R. Heid, K.-P. Bohnen, and B. Renker, *Adv. Solid State Phys.* **42**, 293 (2002); R. Heid, B. Renker, H. Schober, P. Adelmann, D. Ernst, and K.-P. Bohnen, *Phys. Rev.* **B67**, 180510 (2003).
49. Takashi Aizawa, Wataru Hayami, and Shigeki Otani, *Phys. Rev.* **B65**, 024303 (2001).
50. N.L. Bobrov, P.N. Chubov, Yu.G. Naidyuk, L.V. Tyutrina, I.K. Yanson, W.N. Kang, Hyeong-Jin Kim, Eun-Mi Choi, C.U. Jung, and Sung-Ik Lee, in: *New Trends in Superconductivty*, Vol. 67 of NATO Science Series II: *Math. Phys. Chem.*, J. F. Annett and S. Kruchinin (eds.), Kluwer Acad. Publ. (2002), p. 225 (see also: *cond-mat/0110006*).
51. A.A. Golubov, J. Kortus, O.V. Dolgov, O. Jepsen, Y. Kong, O.K. Andersen, B.J. Gibson, K. Ahn, and R.K. Kremer, *J. Phys.: Condens. Matter* **14**, 1353 (2002).
52. Yu.G. Naidyuk, I.K. Yanson, O.E. Kvitnitskaya, S. Lee, and S. Tajima, *Phys. Rev. Lett.* **90**, 197001 (2003).
53. I.O. Kulik, *Fiz. Nizk. Temp.* **18**, 450 (1992) [*Sov. J. Low Temp. Phys*. **18**, 302 (1992)].
54. A.E. Koshelev and A.A. Golubov, *Phys. Rev. Lett*. **90**, 177002 (2003).